Journal of
Engineering Sciences
Faculty of Engineering
Assiut University
JES
مجلة
العلوم الهندسية
كلية الهندسة
جامعة أسيوط
journal homepage: http://jesaun.journals.ekb.eg

Production of externally gear parts with a new multi-level forming tool based on rotary ballizing technology using Numerical and experimental study

Received 30 January 2025; Revised 23 April 2025; Accepted 26 April 2025

Hammad T. Elmetwally [1]
Emad A. Fahmy [2]
Eman S. M. Abd-Elhalim [3]
Mohamed N. El-Sheikh [4]
Ahmed M.I. Abu-Oqail [5]
Ayman Ali Abd-Eltwab [6]

Keywords
Multi-stage ballizing; Externally gear parts; mathematical model; shear spinning; Process parameters

Abstract: External gear components are used in a variety of production and manufacturing areas, including motion, energy, and power transmission in many industrial applications. Examples include transportation equipment, aerospace equipment, and machine tools such as lathes and milling machines, all of which rely on gearboxes. As a result, these components are receiving increasing attention. This paper introduces an innovative multi-level rotary ballizing technique for manufacturing toothed tubular parts in one stroke. The process was examined both experimentally and numerically. The experimental study focused on key parameters, including die rotational speed (100, 200, 315, and 400 rpm), mandrel axial feed rate (0.13, 0.15, 0.18, and 0.21 mm/rev), and cross-feed values (4.5, 5.5, and 6.5 mm), achieved using three levels of ball. Additionally, initial tube thicknesses of 6, 7, and 8 mm were analyzed. The study investigated the influence of these parameters on forming load, filling ratio, and the hardness of the formed product. The results demonstrated that these factors significantly impact forming load, filling ratio, and overall product quality. A mathematical model was developed to predict forming loads numerically, and the calculated results showed a strong correlation with experimental findings. Moreover, the experimental results confirmed the effectiveness of the proposed multi-level ballizing technique in successfully forming toothed parts with greater thicknesses while significantly reducing forming loads compared to the single level ballizing method.

1. Introduction

Power is usually transmitted by a number of metros, including belts and gears. Gears and toothed parts are important and indispensable parts in practical industrial life because they are essential components relied upon in all areas of manufacturing and production, including the military industry, the aerospace industry, and workshops operating all types of machinery. No machine is complete without a gear box. This is because gear boxes are

[1] Mech. Dep., Faculty of Technology and Education, Beni-Suef University, Beni-Suef, Egypt. memo_power2003@yahoo.com
[2] Mechanical Dep., Faculty of Technology and Education, Beni-Suef University, Beni-Suef, Egypt. emadfahmy300@gmail.com
[3] Mechanical Eng. Dep., Faculty of Engineering, Assiut University, Assiut, Egypt. eman_sayed@aun.edu.eg
[4] Mechanical Dep., Faculty of Technology and Education, Beni-Suef University, Beni-Suef, Egypt. elshikh53@yahoo.com
[5] Mechanical Dep., Faculty of Technology and Education, Beni-Suef University, Beni-Suef, Egypt. AbuOqail@yahoo.com
[6] Assoc. Professor, Mechanical Engineering Department, Faculty of Engineering, Beni-Suef University, Beni-Suef, Egypt. AymanAli@eng.bsu.edu.eg

https://doi.org/10.21608/jesaun.2025.356763.1416

unique in that they transmit motion and power without slipping (without losing power or speed). In light of the tremendous and rapid technical progress in this era, the methods of manufacturing gears or toothed tubular parts in general have developed and been transformed from traditional methods such as: milling, hobbing machines, and others, to different, Innovative forming methods. It is well known that forming processes generally differ from machining and cutting processes in the following: In forming processes, the amount of metal waste is minimal, approximately 10%, while in machining processes, and waste due to chip removal can reach 60% of the mass of the raw materials used. In forming processes, mechanical properties are improved, while in cutting processes, the mechanical properties of the product remain unchanged. Forming processes are widely used, especially for products with complex shapes, while cutting processes are difficult to manufacture, as they require high technical skills and expensive manufacturing machines. Consequently, production costs in forming processes are lower than in machining processes. Production rates in forming processes are also high, while in cutting processes, production rates are expensive, and production rates are low. Many previous studies were conducted to produce internally splined tubes. The ballizing process enhances the hardness of the pre machined holes. Beyond hole sizing and surface improvement, ballizing has a wide range of applications, some of which are difficult or impossible to achieve with other methods. An AISI 1020 steel workpiece was manufactured using a multi-pass single-roller flow forming process over a splined tool. The findings indicate that the highest measured equivalent true plastic strain was situated at the interface of the workpiece and mandrel. It is noteworthy that as the reduction in workpiece thickness increased, the ultimate equivalent plastic true strain near the workpiece, especially near the base of the inner ribs, also showed an increase [1]. The process involving the displacement of material from one area on the surface to another usually results in the formation of a topography characterized by three distinct layers. Another category of processes yielding similar three-layered topographies involves the addition or removal of material, both above and below the initial surface's average line. In instances of material addition, the resulting topography conforms to the SRR pattern, as peaks are introduced concurrently with the filling of cavity. Conversely, in cases of material removal, the resulting topography follows the RSS pattern, as valleys are augmented simultaneously with the removal of peaks [2]. Utilizing micrography analysis has proven instrumental in enhancing our comprehension of metal plastic flow during the process of rearward ball spinning for fluffy-walled tubular components featuring longitudinal internal ribs. Multi-pass spinning leads to material work hardening, detrimentally affecting the formability of inner ribs. The grain orientations indicate that the metal follows tangential and radial directions as it flows into the mandrel grooves. These simulations highlight that the three components of the spinning force increase as the number of spinning passes increases, which means that hardening occurs in the metal throughout the multi-stroke spinning process [3]. Empirical investigations demonstrated a distinct influence of feed ratio and spindle speed on critical factors such as internal diameter, wall thickness, and load demands. Notably, using lower feed rates and higher speeds of the spindle resulted in a significant expansion of the inner diameter and a reduction in wall thickness. Furthermore, elevated spindle speeds were particularly impactful in substantially diminishing the forming load requirements. The material's hardness exhibited a direct correlation with the extent of thickness reduction in the annealed state [4]. Employing a rounded corner design in the transition region between the teeth and grooves results in minimal fluctuations in metal flow and contact force. This design alteration proves advantageous in mitigating defects and averting mandrel failure [5]. A new analytical approach was introduced to determine the optimal angle of attack for tube spinning, with the main objective of minimizing the spinning load. It was found that the optimal angle of attack be calculated numerically by the supreme equation [6]. During the production of thin-walled tubes with small diameters using Ball spinning. Was a critical concern in this process is the potential occurrence of a peeling phenomenon, which arises when factors like the working angle are not suitably chosen. This phenomenon can lead to deformations such as material crashing, curling, and unwanted coverage over areas preceding the ball, sometimes resulting in damage to the working die. It is concluded that peeling arises when the actual working angle surpasses a critical value αc. Conversely, if the actual running angle is lower than or equal to αc, the material in forefront of the ball's flows smoothly. [7] During the backward ball spinning process. Experimental findings indicated the presence of a minimum ball diameter essential for ensuring the proper formation of internal ribs. The minimum achievable diameter is influenced by factors such as feed ratio, wall thickness reduction, initial tubular blank thickness, and material properties. In the backward ball spinning process for thin-walled tubular components with longitudinal inner ribs, ball size plays a crucial role. It significantly affects the magnitude of the spinning force and various quality aspects of the part, including surface finish, material flow stability, and inner rib formation. Larger ball sizes help minimize surface buildup while enhancing inner rib height [8]. The relationship between ball size, axial feed, and the number of balls is critical in determining the final surface quality of the produced parts. Additionally, the configuration and dimensions of the contact surface between the ball and the workpiece directly affect the deformation force components [9]. During backward ball spinning of thin-walled tubular parts with longitudinal inner ribs, the deformation zone is in a three-dimensional compressive stress state. In the inner rib region, tensile strain occurs in the radial and axial directions, while compressive strain occurs in the tangential direction. On the other hand, in the adjacent wall deformation zones, compressive strain occurs in the radial direction and tensile strain occurs in the axial and tangential directions. Moreover, all three spinning force components increase as the ball stroke increases, with the radial force component being the highest, while the tangential force component remains the lowest [10-13]. To enhance groove height, employing large thickness reduction and feed rate is recommended. [14] The significant influence of two main parameters, namely workpiece diameter rate and feed ratio (v), on the behavior observed in ball rotation operations must be considered [15]. During ball spinning to form inner-grooved copper tubes, simulation results have shown that folding defects arise due to the gap between the inner surface of the copper tube and the plug. To mitigate these defects, several measures have been proposed based on finite element simulations. These include minimizing the difference between the inner diameter of the reduced blank tube and the outer diameter of the plug, incorporating appropriate rounded corners between the groove wall of the plug and its outer surface, and reducing the roughness of both the plug's groove walls and outer surface. Microstructural analysis of the cross-section of copper tubes reveals that folding defects result from multi-track metal flow during the spinning process [16]. During the ball spinning of fluffy-walled tubular parts, all three force components increase as the feed ratio and ball diameter increase. Moreover, in backward ball spinning, each spinning force component is significantly higher than its corresponding force in forward ball spinning [17]. A novel ball set design has been introduced to tackle various challenges in the tube spinning process, including material build-up in front of the forming balls, material folding on the tube's internal surface, and potential mandrel failure due to load fluctuations at the root of the forming teeth. The new design incorporates smaller ball sizes compared to conventional designs, making it more suitable for tubes with relatively small thicknesses.[18] pipe spinning utilizes a functionally graded ballizing arrangement. The proposed design features four balls, each positioned on a separate plane. This novel configuration has demonstrated significant potential in mitigating accumulation formation in front of the forming balls, particularly at specific ball arrangements. [19] The maximum value of strain hardening in-creased with both interference and wall thickness. The greater the wall thickness, the lower the wall elasticity. [20] At surface roughness increases, fatigue life tends to decrease notably. When comparing equal surface roughness conditions, it was observed that ballizing yielded the shortest fatigue life for Assab 760 steel, while polishing resulted in the longest stress life. The reason behind the reduced stress life in the case of ballizing can be attributed to a decline in the material's fatigue resistance when subjected to a certain level of pre-strain. [21] It was established that smaller ball diameters result in higher levels of stress and strain, along with in-creased strain rates. Numerical analysis further reveals that the reduction rate plays a significant role in shaping the strain state within the inner tube holes after the ballizing process. [22, 23] There exists a critical interference value that maximizes the improvement in microhardness, roundness, and surface finish during the ballizing process. The ballizing process yields favorable surface characteristics, significantly enhancing the average surface roughness by approximately 85%. Moreover, it has a positive impact on the bearing ratio. Precise control over surface characteristics can be achieved by carefully adjusting the interference parameter. [24] Generally, increasing the interference (the gap between the ball tool and the bore) enhances surface quality up to an optimal point. However, excessive interference may cause micro-profile distortion and excessive work hardening, leading to a deteriorated surface finish. Additionally, higher interference levels result in an increased average outer surface strain. Surface hardness improves with greater rotational speed, feed rate, and depth of penetration, which positively contributes to the overall effectiveness of the process [25, 26] it was observed that the attack angle produced the smallest magnitude of axial force, which also resulted in the least amount of material accumulation. [27] The material displaced by the ball can be categorized into three components: elastic displacement, plastic displacement, and material compressibility. [28] The ballizing load was predicted under both dry and lubricated conditions, assessing the effectiveness of various common lubricants and comparing them in terms of load reduction and their impact on surface finish. It was found that predicting the load during ballizing without lubrication is straightforward, but when lubricants are applied, the prediction becomes more challenging due to the unknown value of "β", which represents the fraction of the load-supporting area where film breakdown occurs. This value is crucial for evaluating the performance of a specific lubricant. Among the lubricants tested, a soap solution was found to be the most effective. While lubrication reduces friction, it also diminishes the finish improvement achieved through metallic contact and the burnishing effect between the ball and the workpiece. [29] The ideal length-to-diameter ratio for a ballizing tool should range from 1/10 to 10 times the hole diameter. Additionally, the wall thickness of the material should be at least greater than 1/10th of the hole diameter. The ballizing tool should not have a hardness exceeding 45 Rockwell scale, while the balls used should have a hardness greater than 65 Rockwell scale [30,31] Durin the flow forming procedure used on a lathe to manufacture internal gears. It was discovered that all factors and their interactions impact tooth height, including the attack angle, thickness reduction, the relationship between roller diameter and attack angle, as well as the interaction between roller diameter and feed rate. [32] Innovative "symmetric cold expansion" method offers superior control and uniformity of residual stresses, as well as proven enhancements in fatigue life through experimental validation. [33] To achieve the specified final diameter, an oversized ball must be employed, and the extent of oversizing can be estimated from the recovery angle value. Surface hardness increased by approximately 20% in most specimens, and this increase was more pronounced with greater interference. [34] Generally, rising the interference improves sur-face quality up to an optimal point, beyond which it begins to decline. This is because the ballizing process involves plastic deformation, and insufficient interference may result in only elastic deformation, leading to poor quality, particularly at small interferences. On the other hand, excessive interference can cause micro-profile distortion and excessive work hardening, leading to poor surface finish. [35, 36] The ballizing process is effective for finishing mated holes, even those with slight bends or s-bends, in a single pass. It can handle interrupted areas, such as cross holes and recesses, without difficulty. Ballizing is versatile and can be applied to various materials, including ferrous, non-ferrous, and stainless steel. But it not suitable for materials that have been hard chromium plated. Heat treatment carried out after Ballizing can disrupt adjust the dimensions and finishing of the ballizing tool, so it should be considered when planning the manufacturing process. [37] During the ball-shaped spinning process for manufacturing internally-splined tubes, key variables such as mandrel rotational speed, axial feed, and cross in-feed were found to significantly affect both the forming load and the quality of the formed sleeves. The rough surface of the sleeves decreases as the cross in-feed increases, while it increases with higher axial feed. Additionally, the filling ratio improves with an increase in both cross-in-feed and axial feed. [38] The Design of Experiments technique was applied, revealing that speed and feeding are the most critical variables influencing power consumption. The resulting force on the roller is governed by factors such as the roller attack angle, roller nose radius, and reduction per-centage. The resultant force is composed of three components: axial, radial, and circumferential forces. Among these, axial force is the largest, followed by radial force, while the circumferential force is the smallest. [39]. in general, in studying the variables of manufacturing processes of a raw material or product, Mahmoud Hashem et al. used the ANOVA package for this purpose [40-43], Other references have provided methods for selecting experimental/operational parameters, composite properties, dynamic parameters, finite element analysis, numerical simulation, etc. [44-49]. Jena, P. C. et al. used dynamic analysis of FRP cracked beams using neural network. [50]. References introduced processing technology's fault crack assessment by FEM of AMMC beam produced by many methods such as modified stir casting method.

It can be seen from the previous review that the process of forming the gear needed more investigation. Here, we propose rotary forming with balls (balling process) to produce gears. This paper proposes a new method of forming toothed parts by rotational ballizing process using a new tool. In this research suggests a novel design that promises to address all these problems simultaneously using simple tools to produce external gears or any other externally toothed parts. In addition to the formation of tubular sections with relatively large thicknesses compared to previous studies in the spinning of internally splined or non-splined tubes. Also, analytical and practical work is done to examine the formation of externally toothed components utilizing a new rotating ballizing approach.

2. Numerical analysis of the single stage ballizing technique

Given the experimental data in Table 1, consider the problem of estimating the value of the function at non-tabulated points. Figure 1 is a graph of the values in Table1. Table. 2 show the data to fitting curve. From this graph, the actual relationship between x and y appears to be a straight polynomial line. The lack of a line that exactly matches the data is probably due to errors in the data. Therefore, it is unreasonable to expect the approximate function to match the data exactly. In fact, such a function would result in oscillations that do not exist as they should. For example, the graph of the interpolating polynomial of 2-degree equation shown in unbounded mode for the data in Table 3.

3. Polynomial Least Squares for Numerical forming load

The general problem of approximating a set of data, $\{(x_i, y_i), i = 1, 2, m\}$, with an algebraic polynomial in general form as the following

$$P_n(x) = y = a_n x^n + a_{n-1}x^{n-1} + \cdots + a_1 x + a_0 \tag{1}$$

The polynomial of degree in < m − 1, using the least squares procedure is handled similarly. We choose the constants $a_0, a_1, \ldots. and\ a_n$ to minimize the least squares error E = E_2 ($a_0, a_1, \ldots. and\ a_n$), where

$$E = \sum_{i=1}^{m} (y_i - P_n(x_i))^2 \quad (2)$$

$$= \sum_{i=1}^{m} (y_i)^2 - 2\sum_{i=1}^{m} P_n(x_i) y_i + \sum_{i=1}^{m} (P_n(x_i))^2 \quad (3)$$

$$= \sum_{i=1}^{m} (y_i)^2 - 2\sum_{i=1}^{m} \left(\sum_{j=0}^{m} a_j (x_i{}^j)\right) y_i + \sum_{i=1}^{m} \left(\sum_{j=0}^{m} a_j (x_i{}^j)\right)^2 \quad (4)$$

As in the linear case, for E to be minimized it is necessary that ∂E/∂aj = 0, for each j = 0, 1, n. Thus, for each j, we must have

$$0 = \frac{\partial E}{\partial a_j} = -2\sum_{i=1}^{m} \left(\sum_{j=0}^{m} y_i (x_i{}^j)\right) + 2\sum_{i=1}^{m} a_k \sum_{j=0}^{m} (x_i{}^{j+k}) \quad (5)$$

This gives n + 1 normal equations in the n + 1 unknown's aj. These are

$$\sum_{k=0}^{n} a_k \sum_{i=1}^{m} (x_i{}^{j+k}) = \left(\sum_{i=1}^{m} y_i (x_i{}^j)\right) \quad (6)$$

For each j = 0, 1, . . ., n. and for it is helpful to write the equations as follows:

$$a_0 \sum_{i=1}^{m} x_i{}^0 + a_1 \sum_{i=1}^{m} x_i{}^1 + a_2 \sum_{i=1}^{m} x_i{}^2 + \ldots\ldots + a_n \sum_{i=1}^{m} x_i{}^n = \sum_{i=1}^{m} y_i\, x_i{}^0 \quad (7)$$

$$a_0 \sum_{i=1}^{m} x_i{}^1 + a_1 \sum_{i=1}^{m} x_i{}^2 + a_2 \sum_{i=1}^{m} x_i{}^3 + \ldots\ldots + a_n \sum_{i=1}^{m} x_i{}^{n+1} = \sum_{i=1}^{m} y_i\, x_i{}^1 \quad (8)$$

… …… …… …… …… ……. …

$$a_0 \sum_{i=1}^{m} x_i{}^n + a_1 \sum_{i=1}^{m} x_i{}^{n+1} + a_2 \sum_{i=1}^{m} x_i{}^{n+2} + \ldots\ldots + a_n \sum_{i=1}^{m} x_i{}^{2n} = \sum_{i=1}^{m} y_i\, x_i{}^n \quad (9)$$

Least squares polynomial

$$f(x) = y = a_0 + a_1 x + a_2 x^2 \quad (10)$$

Fit the data in the following Table 1 with the discrete Least Square Polynomial of degree at most 2, where $\mathbf{n = 2, m = 9}$ **and** $y = f(x) = a_0 + a_1\, x + a_2\, x^2$

$$m a_0 + a_1 \sum_{i=1}^{m} (x_i) + a_2 \sum_{i=1}^{m} (x_i{}^2) = \sum_{i=1}^{m} (y_i) \quad (11)$$

$$a_0 \sum_{i=1}^{m} (x_i) + a_1 \sum_{i=1}^{m} (x_i{}^2) + a_2 \sum_{i=1}^{m} (x_i{}^3) = \sum_{i=1}^{m} (x_i\, y_i) \quad (12)$$

$$a_0 \sum_{i=1}^{m} (x_i{}^2) + a_1 \sum_{i=1}^{m} (x_i{}^3) + a_2 \sum_{i=1}^{m} (x_i{}^4) = \sum_{i=1}^{m} (x_i{}^2 y_i) \quad (13)$$

Table 1 the forming load values against die rotating speed, N (rpm)

i	1	2	3	4	5	6	7	8	9
N(rpm)	50	63	80	100	125	160	200	250	315
$\mathbf{F_t}$ (KN)	3.5992	6.9625	5.0810	5.3344	3.9081	3.1865	2.9079	2.8655	2.7327

From the data tabulated in Table 2 can be calculated the following equations

eq14 $9a_0 + 1343a_1 + 265819a_2 = 36.57824$ **(14)**

eq15 $1343a_0 + 265819a_1 + 62817047a_2 = 4715.697$ **(15)**

eq16 $265819a_0 + 628170475a_1 + 16414314211a_2 = 831709.7$ **(16)**

Table 2 the data to fitting curve for forming load

m	x_i N	y_i F_t	$x_i^{\ 2}$	$x_i^{\ 3}$	$x_i^{\ 4}$	$x_i\ y_i$	$x_i^{\ 2}\ y_i$
1	50	3.5992	2500	125000	6250000	179.961	8998.05
2	63	6.9625	3969	250047	15752961	438.6408	27634.37
3	80	5.0810	6400	512000	40960000	406.4827	32518.62
4	100	5.3344	10000	1000000	100000000	533.4483	53344.83
5	125	3.9081	15625	1953125	244140625	488.5141	61064.26
6	160	3.1865	25600	4096000	655360000	509.849	81575.84
7	200	2.9079	40000	8000000	1600000000	581.5903	116318.1
8	250	2.8655	62500	15625000	3906250000	716.3965	179099.1
9	315	2.7327	99225	31255875	9845600625	860.8144	271156.5
Σ	1343	36.57824	265819	62817047	16414314211	4715.697	831709.675

To solve this equations system (eq No 14-16) using Maple, we first define the equations And then solve the system with
Solve ({eq1 No 14, eq2 No 15, and eq3 No 15}, {a0, a1, a2}) this gives

$a_0 = 6.650336$ **(17)**

$a_1 = -0.024916$ **(18)**

$a_2 = 3.8325\mathrm{E} - 05$ **(19)**

Thus, the forming load or least squares polynomial of degree 2 fitting the data in Table 3 is

$f(x) = y = a_0 + a_1 x + a_2 x^2$ **(20)**

$y = f(x) = 6.650336 - 0.024916x + 3.8325\mathrm{E} - 05x^2$ **(21)**

Whose graph is shown in Fig. 1? At the given values of xi we have the approximations shown in Table 3 and 4.

Table 3 the data to fitting curve for numerically and experimentally forming load with the Errors at all points

i	1	2	3	4	5	6	7	8	9
x_i (N)	50	63	80	100	125	160	200	250	315
y_i (F_t)	3.599	6.962	5.081	5.334	3.908	3.186	2.907	2.865	2.732
$P(x_i)$	5.500	5.232	4.902	4.541	4.134	3.644	3.200	2.816	2.604
$y_i - P(x_i)$	-1.901	1.729	0.178	0.792	-0.226	-0.458	-0.292	0.048	0.128
E%	-10.178	12.239	3.516	14.856	-5.796	-14.383	-10.047	1.707	4.689

The total error, E = 0.3928655 (-3.3970894 %)

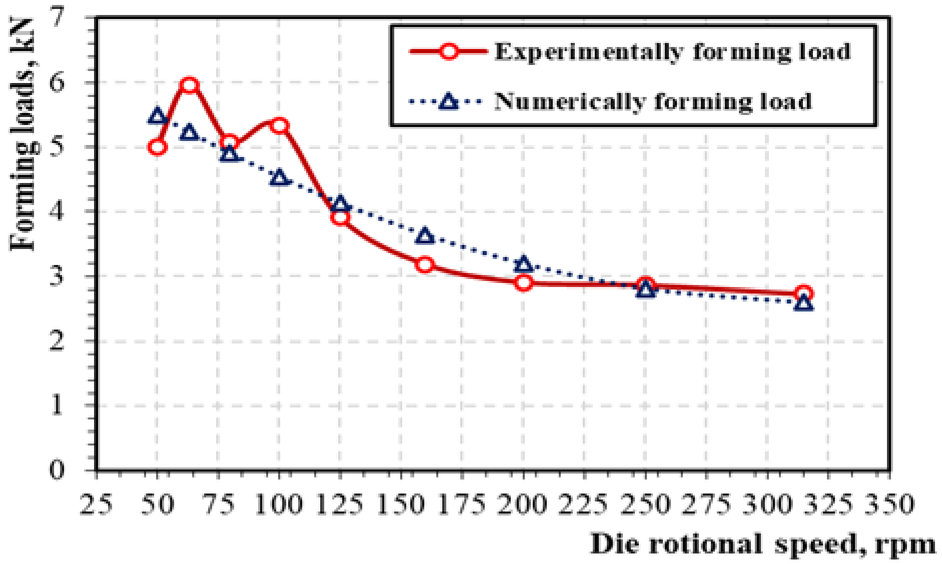

Fig. 1 A comparison between computed Numerically and Experimentally forming load results data at axial feed 0.15 mm/rev.

4. EXPERIMENTAL WORK

The multi-stage ballizing depends on dividing the thickness of the metal required to be displaced (flowed) inside the cavity of the die teeth into layers that correspond in number to the stages of the ball used, so that the graduated outer diameters of the ball together give a streamlined conical shape, for easy displacement of the metal and the transition of flow from one stage to another gradually with High flexibility.as shown as in **Fig. 2** , and therefore all common ballizing problems such as metal piling up in front of the forming balls, folding, radial and axial load swing result from the metal piling up, are overcome. In addition to overcoming the elastic spring of the metal behind the forming balls in a relatively large amount compared to single- stage ballizing, and the metal peeling phenomenon. All that at one time (in one stroke). This gives the possibility of obtaining the externally toothed parts with greater thicknesses, speed in forming, saving time, reducing the forces consumed more, and ensuring complete filling of the product teeth. In addition to improving the mechanical properties of the product, such as hardness and others. **Fig. 3** They explain schematic drawing of multi-stages ballizing process sequence and isometric section of the process and sample ejection mechanism.

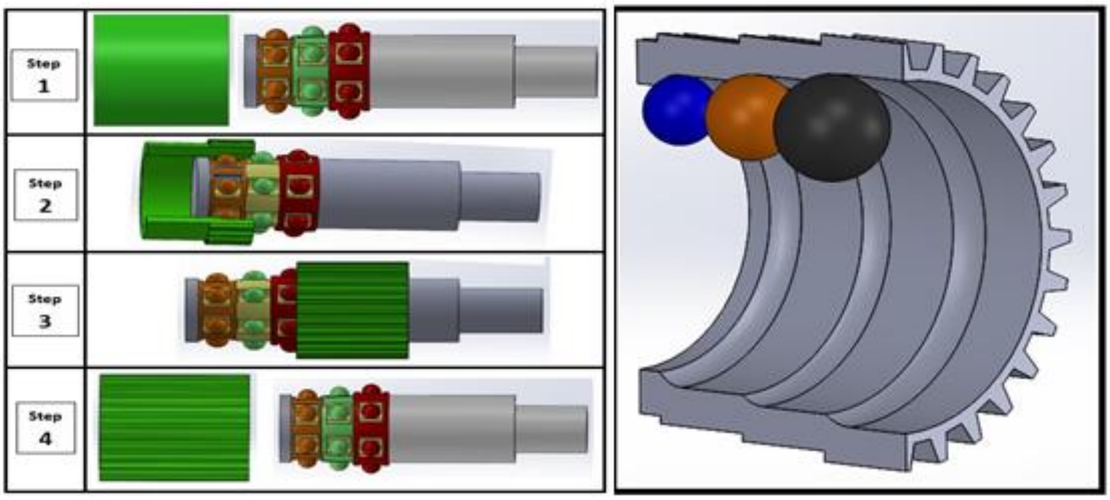

Fig. 2 Isometric section showing multi-stage ballizing process and sample ejection

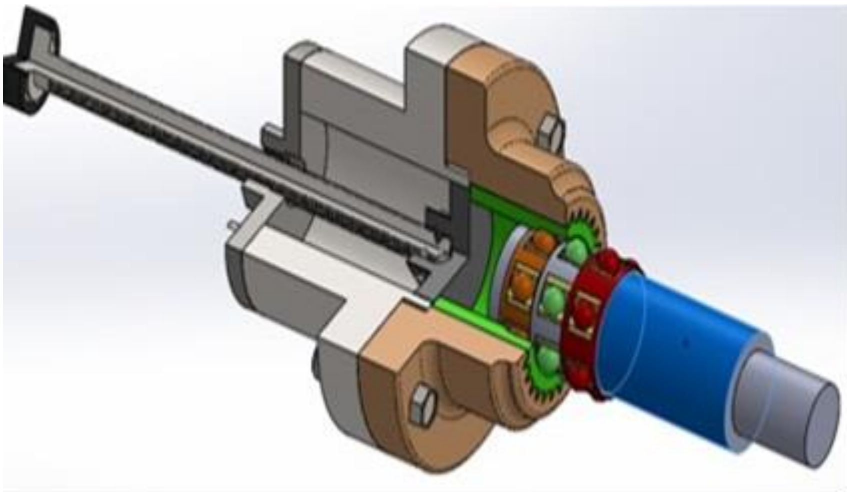

Fig. 3 Isometric section showing multi-stage ballizing process and sample ejection

4.1 Experimental set-up of the multi-stages rotating ballizing technique

Figure 4 Shows the components of the testing device used in the forming process. The proposed design of the forming tool is a mandrel mounted on it two level ball or three level with graduated outer diameters (multi-stage ballizing process) and each ball bearing has six rotating forming balls with diameters of 13, 14 and 16 mm, respectively. The balls are made of hardened tool steel and are spaced 60 degrees apart to prevent folding of the metal during forming. They were designed to eliminate all the known problems of the ballizing process, which faced many researchers in previous studies, and still are still such as piling up, folding and others. **Fig. 5** shows a schematic diagram of the forming tools used to form the toothed parts externally (in one stroke) using the multi-stage pelleting technique. The forming die rotates at the speed of 315 rpm obtained from process parameters for single stage ballizing, while the rotating forming balls rotate almost at the same speed as the toothed die when it comes into contact with the workpiece placed inside the toothed die. The radial feed of forming balls ranges between (5.5 mm and 6.5 mm). The cross in-feed value (interference between the forming balls and the sample) is changed by changing the inner diameter of the tubular sample while keeping the diameter of the ball bearing constant according to the required diagonal feed value (diagonal interference). The axial feed rate of mandrill was 0.13 mm/rev (also obtained from process parameters for single-stage ballizing). The toothed die is fixed in the lathe chuck at one end and the workpiece is inserted into it at the other end. The die gap provided axial support for the tubular specimen, while the die teeth rotated it. The tubular sample is made of commercial lead, with a strength coefficient of K= 63 MPa and a strain hardening exponent of n=0.149 determined by an experimental pressure test. The lead was bought as scrap, it was melted and purified from impurities. Tubular samples were made by pouring in a metal mold, and the casting mold was devised and produced to make the tubular samples in the required dimensions. The spindle is placed on top of a conventional lathe carriage and is set centrally with the centerline of the lathe using a dial gauge with a sensitivity of 0.01 mm. The forming balls approach the sample from the free side of the mold until contact occurs between them without penetration into the sample, then the speed and axial feed of the machine are adjusted. Automatic feeding has been activated. Thus, the sample rotates with the rotation of the mold, while the forming balls move independently and axially along the surface of the sample from the inside.

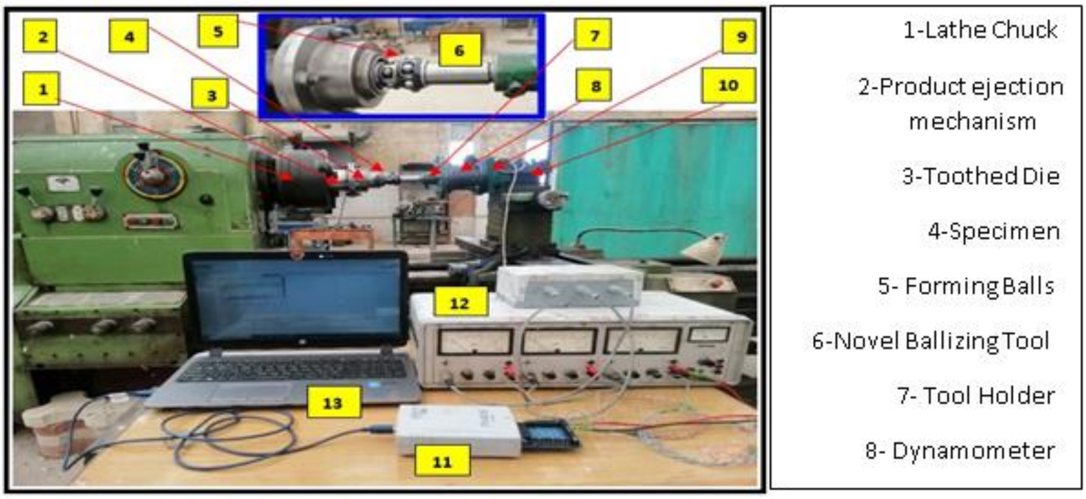

Fig. 4 Experimental set-up of the multi-stage rotating ballizing technique as a novel forming tool

4.2 Force, hardness, and filling ratio measurement devices

The forming loads were measured by the dynamometer relates to data logger device. The data logger is a PIC OLOG 1000 series. The data logger is connected to a laptop computer and receives signals with the Pico-Log program. The hardness of the products was measured with a microhardness tester (Micrometre 2001). The filling ratio was calculated as follows:

1- Theoretical geometry (complete filling) was calculated from the die teeth dimensions.
2- Obtained actual geometry (contour) of formed parts is magnified to a predetermined scale using a microscope to calculate the actual volume filled.
3- The filling rate is computed as the following
A photo scan for the die and formed workpiece is illustrated in **Fig. 6.** The actual and theoretical areas were computed using by AutoCAD program. The ratio is the sum of division of the actual and theoretical values.

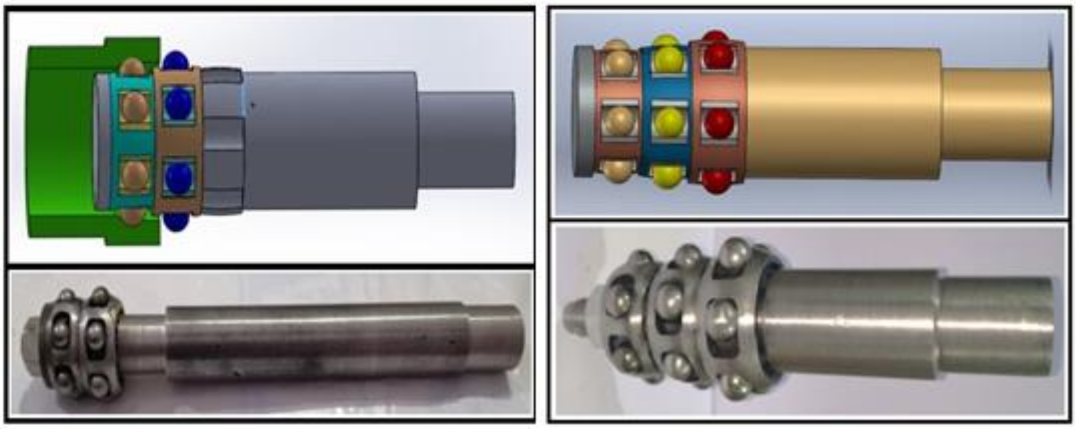

Fig. 5 Schematic diagram showing the two and three-stage mandrel (multi-stages mandrel)

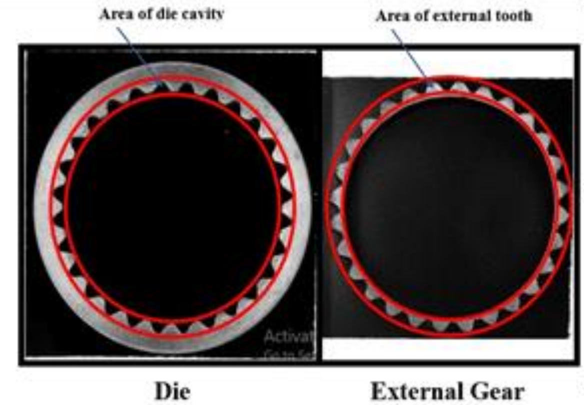

$$FR = \frac{\text{actual volume of external teeth}}{\text{theoretical volume of die cavity}}$$

$$FR = \frac{\text{actual area of external teeth} * \text{tooth length}}{\text{theoretical area of die cavity} * \text{tooth length}}$$

Fig. 6 Photo scan for die and external toothed part to compute the filling ratio.

Experiments were done under optimal conditions derived from single stage ballizing to study the influence of process parameters (t, DT) and machine parameters (f, N) on deformation loads. The influence of process and machine parameters on product quality, defined by hardness and filling rate of the outer teeth of the product, was investigated. Table 2 displays the experimental plan and operational parameters. In this work, experiments were conducted at variable values according to the capabilities available in the experimental machine of test rig, so that a minimum value and maximum values are determined for each variable, and between them, we choose two values. It is known that in determining and designing experiments at the time of the predecessors, such as the Taguchi method, Full and Fractional Factorials and the Optimal design method, experiments are designed for levels with the aim of reducing the number of experiments and thus saving time, effort and cost. Here, in this work, we relied on Full Factorials to design experiments.

5. RESULTS AND DISCUSSIONS

5.1 The geometry of externally toothed components

Figure 7 shows the ball trace geometry for the multi-stage ballizing process, **Fig. 8** Some of the externally toothed tubular products which are produced with the new multistage ballizing technique and **Fig. 9** photo scan for externally toothed tubular products at optimum parameters and different cross-in-feed. It is obvious that the externally toothed tubular product was perfectly manufactured using the innovative multi-stage rotary ballizing technique with thicknesses 7 and 8 mm. This is a novel, simple, and low instrumentation approach.

Fig. 7 shows the ball trace geometry for the multi-stage ballizing process

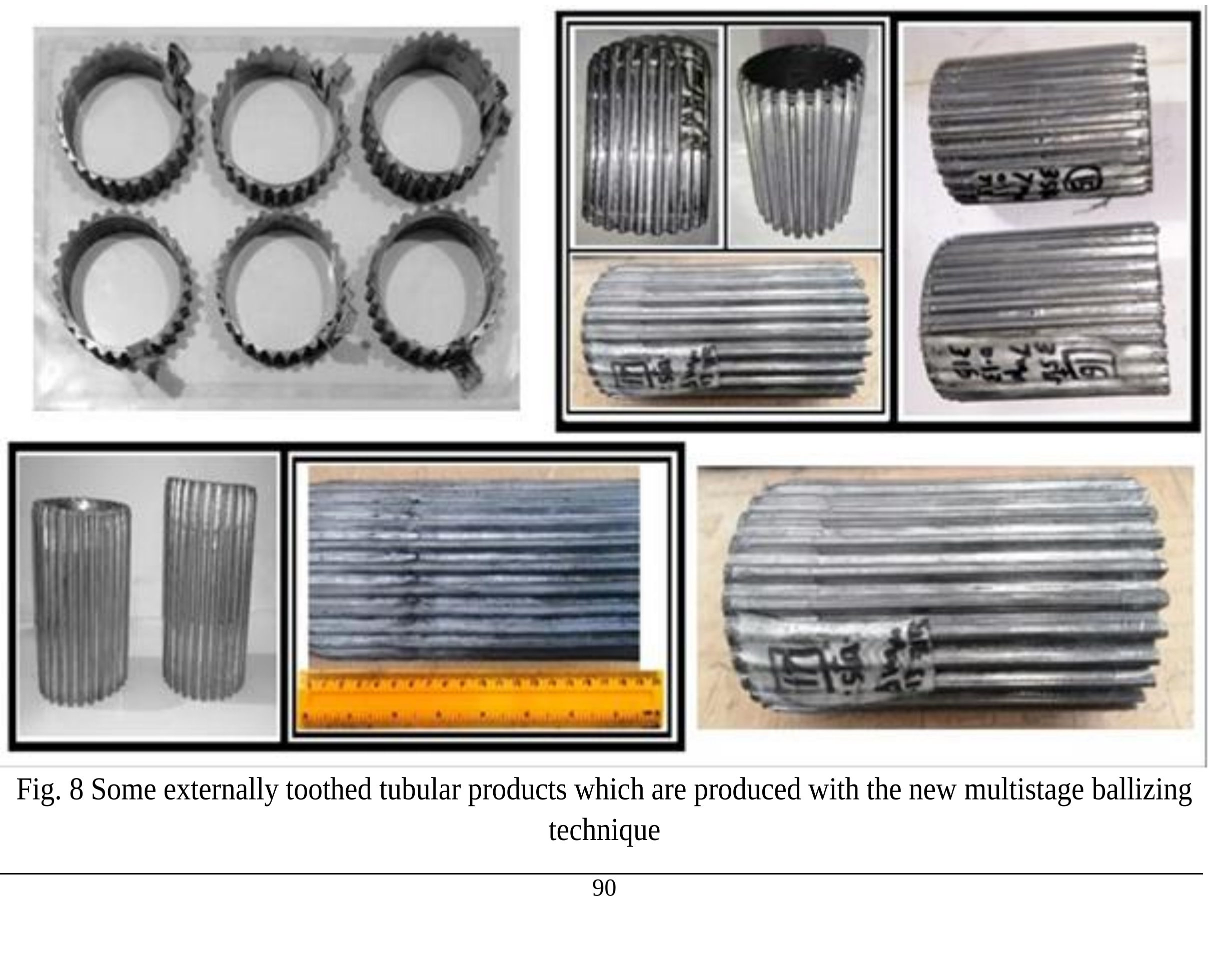

Fig. 8 Some externally toothed tubular products which are produced with the new multistage ballizing technique

Figure 9 shows the teeth filling ratio against die rotational speed. The filling ratio was enhanced by raising the die speed, as illustrated. This is due to increased metal flow caused by greater die rotating speed. Because of a rise in the metal's temperature and flexibility caused by fast friction. Furthermore, as the die rotational speed increases, the forming balls force more metal into the front and inner perimeters of the die, resulting in greater filling for the die tooth cavities.

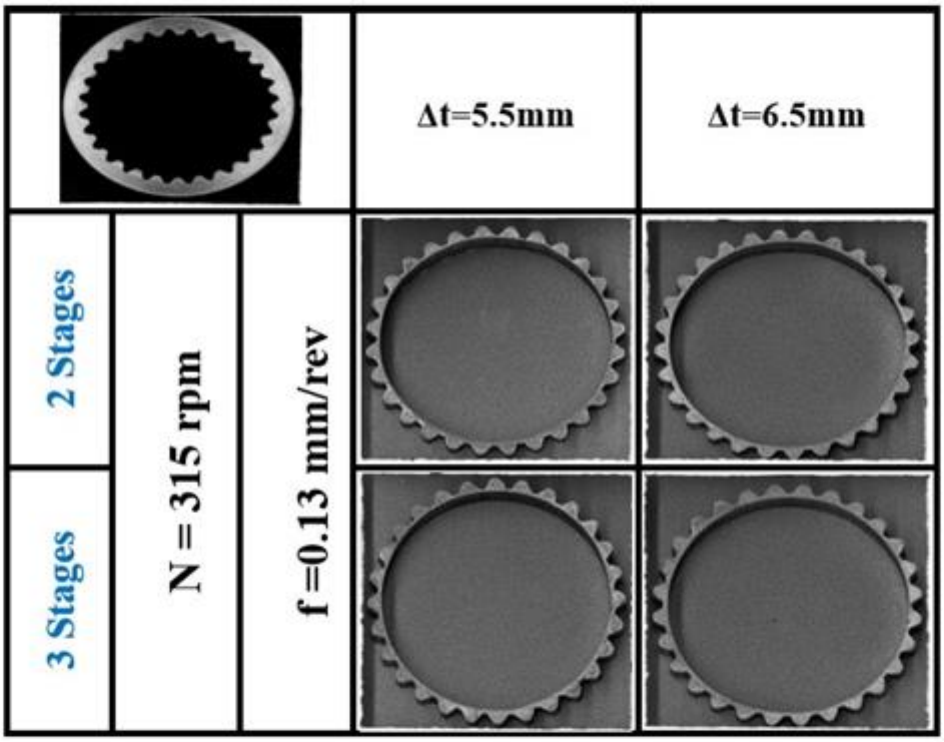

Fig. 9 photo scan for externally toothed tubular products at optimum parameter and different cross in-feed.

5.2 Compare between effects of die rotation speed on resultant forming load with change in the sample thickness.

Fig. 10 shows the relation between die rotation speed and resultant forming load at optimum feed 0.13 mm/rev with different thicknesses (6,7and 8mm). It is clear from the curve that as the thickness of the sample increases with the constant outer diameters of the ball (increasing the interference ratio between the balls and the sample), the forming load rises due to the rise in the contact area. It is also clear that the forming load increases with increasing the speed of the die rotation. This may be due to the increase in the metal accumulated in front of the three levels of ball (increasing the forming rate). The optimum speed is clearly 200 rpm.

5.3 Compare between effect of axial feed with rotational speed on resultant forming load.

Fig. 11 and 12 illustrate the effect of axial feed on the resulting forming load with change in the rotational speed of the die. The forming load increases with increasing axial feed of the mandrel. This is believed to be due to the increased contact area as the axial feed increases, resulting in more buildup and hence a higher forming load.

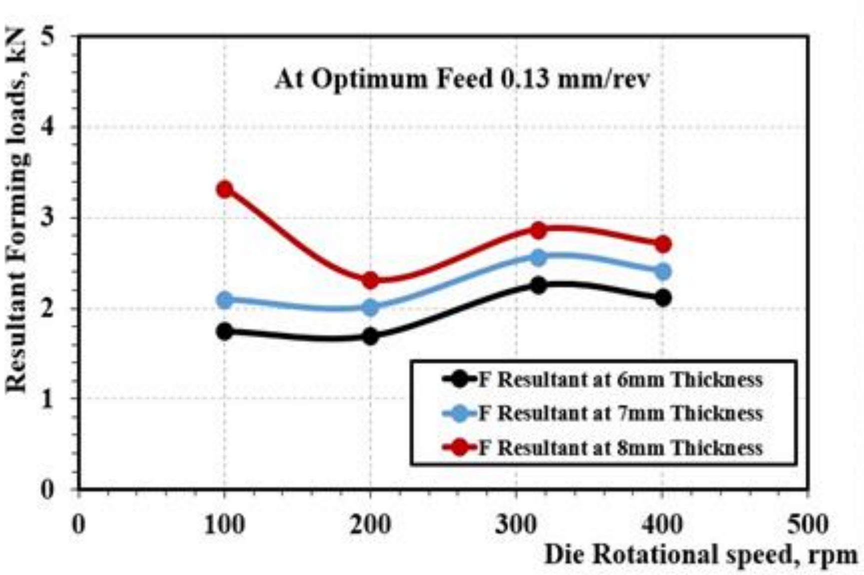

Fig. 10 Impact of die rotation speed on resultant forming load.

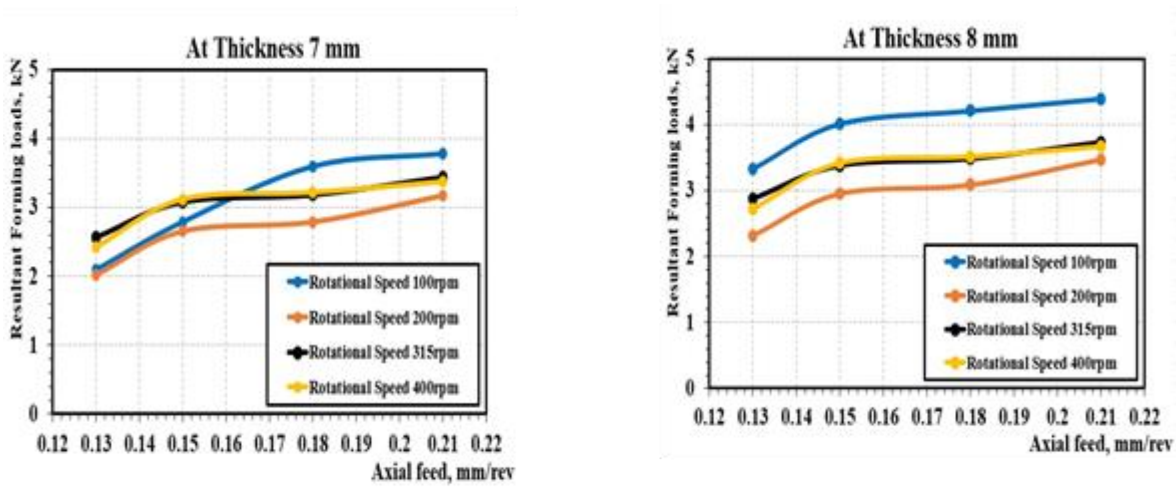

Fig. 11 Impact of axial feed with rotational speed on resultant forming load

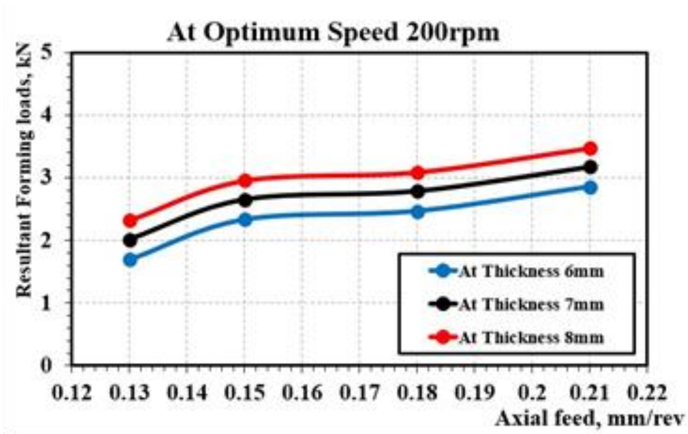

Fig. 12 Compare the effect of axial feed and different thicknesses on resultant forming load at optimum speed 200r.p.m

5.4 Effect of rotational speed and axial feed on tooth filling ratio

Figures (13) illustrates that the filling ratio was enhanced by raising the die speed, as illustrated. It may be due to increased metal flow caused by greater die rotating speed. As a result of a rise in the metal's temperature and flexibility caused by fast friction. Furthermore, as the die rotational speed increases, the forming balls force more metal into the front and inner perimeters of the die, resulting in greater filling for the die tooth cavities. Also increasing the axial feed results in an increased filling ratio, which is believed to be due to the increased contact area between the balls and the sample, displacing more of the accumulated metal to fill the die cavities.

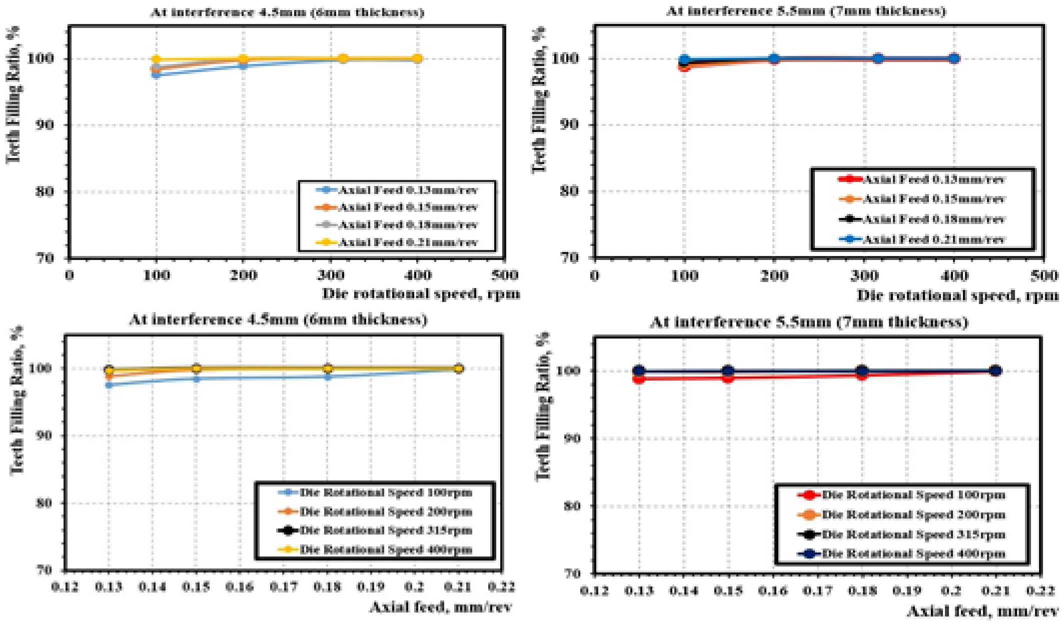

Fig. 13 Effect of rotational speed and axial feed on tooth filling ratio

5.5 Influences of diagonal interference on forming load and the filling ratio

Fig. 14 shows the effect of cross-in-feed on forming load and filling ratio. Forming load increases with increasing cross in-feed, due to increased contact area and accumulated metal. Also, with increasing overlap (cross in-feed), the filling ratio of the die tooth cavities increases. This is believed to be due to the increased contact area between the forming balls and the sample, which leads to an increased amount of displaced metal inside the die cavities. The highest filling ratio of 100% was achieved with 5.5 and 6.5 mm cross-feed at an optimum speed of 315 rpm and an axial feed of 0.13 mm/rev.

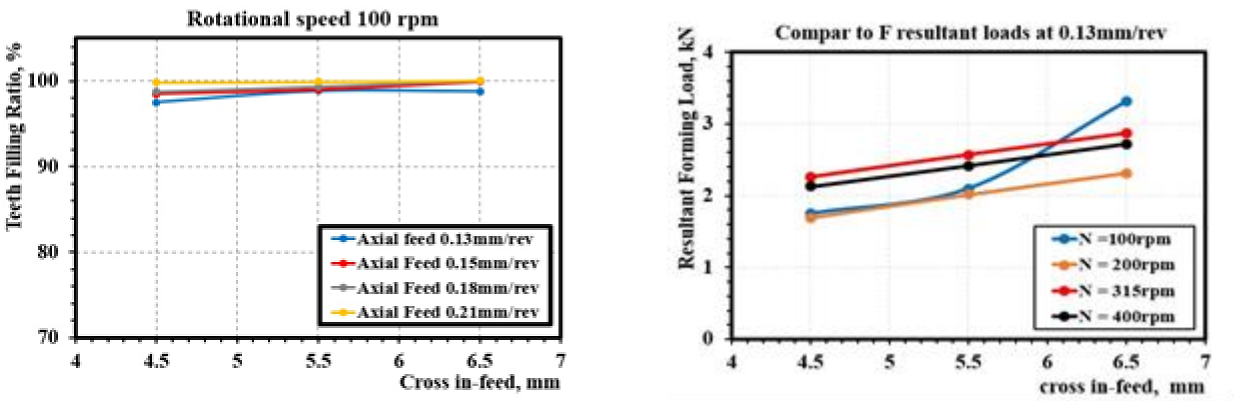

Fig. 14 The relationship between diagonal interference vs filling ratio and forming load

5.6 Impact of rotational speed and axial feed on product hardness.

The findings indicate that an increase in rotational speed leads to greater hardness, attributed to the forming balls repeatedly passing over the same surface area. Conversely, as the axial feed increases, hardness decreases due to the increasing distance between successive ball impacts. This reduces the overall effect of repetitive deformation on the surface of the part. As shown in Fig. 15.

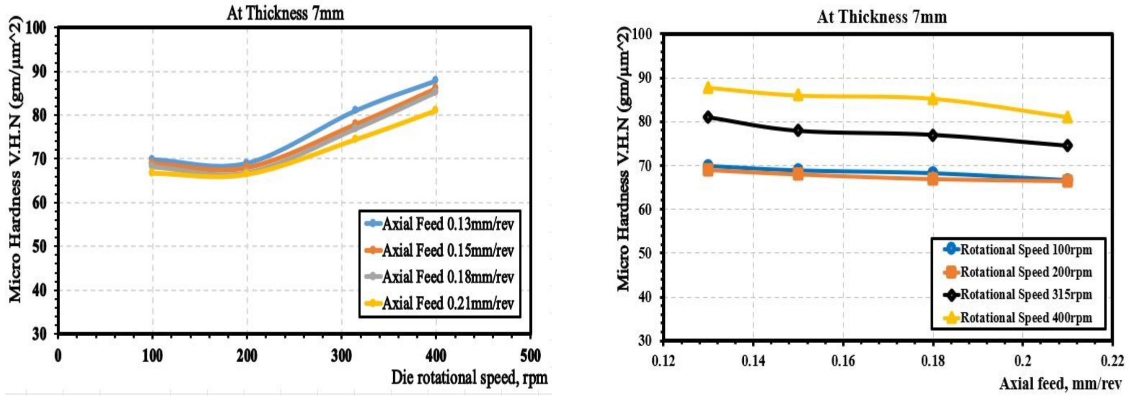

Fig. 15 The relationship between hardness vs dies rotational speed, and axial feed

5.7 Comparison between single-level rotary ballizing process and multi-level rotary ballizing process

Fig. 16 shows the success of the multi-level ballizing process in reducing the forming loads by a large percentage compared to the single level ballizing process due to dividing the formed thickness into several levels of balls and with one tool. With an excellent tooth filling ratio and in one stroke. In addition to enabling the forming of larger thicknesses.

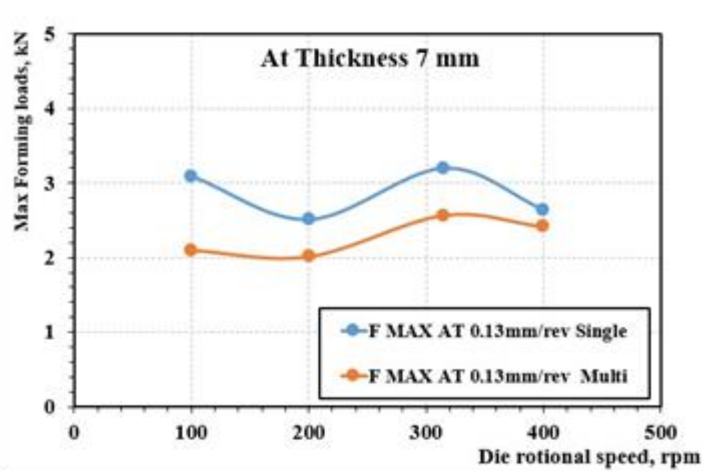

Fig. 16 Comparison between single- stage ballizing process and multi-stage ballizing process

6. CONCLUSIONS

This study concludes that: The multi-stage ballizing process yields excellent results, allowing for thicker tubes and reduced forming load components. The multi-stage ballizing technique was found to significantly reduce metal accumulation on the front of the forming balls by dividing the specimen thickness into three ball stages during forming in a one stroke. Metal folding before and after the forming ball was eliminated, minimizing load fluctuations due to metal accumulation at the front of the ball. Scientific equations were developed to predicted formation loads, and the results were consistent with experiments. The optimum die speed was 315 rpm, and axial feed was 0.13 mm/rev. axial load was the greatest, followed by radial and tangential loads. Ball diameter affects the forming load. As the ball diameter is increased, the forming load increases. Increasing axial feed, speed, and cross-in-feed increases the die filling rate. Hardness increases with increasing speed and cross feed but decreases with increasing axial feed. Agreement between numerical and experimental results.

Acknowledgments

I would want to thank and appreciate the Faculty of Technology and Education at Beni Suef University. I would also want to thank Professor Dr. Muhammad Najeeb El-Sheikh for his continuous support and encouragement throughout my research journey.

Author Contributions:

Funding: This research received no external funding.

Conflicts of Interest: The authors declare no conflict of interest.

Availability of data and materials and Consent for publication: Not applicable

References

[1] Haghshenas, M., Jhaver, M., Klassen, R. J., & Wood, J. T. (2011). Plastic strain distribution during splined-mandrel flow forming. Materials & Design, 32(6), 3629-3636.

[2] JIANG, S. Y., ZHENG, Y. F., REN, Z. Y., & LI, C. F. (2009). Multi-pass spinning of thin-walled tubular part with longitudinal inner ribs. Transactions of Nonferrous Metals Society of China, 19(1), 215-221.

[3] Miscandlon, J., Tuffs, M., Halliday, S. T., & Conway, A. (2018). Effects of flow forming parameters on dimensional accuracy in Cr-Mo-V steel tubes. Procedia Manufacturing, 15, 1215-1223.

[4] Li, Y., Xu, Z., Tang, Y., & Zeng, Z. (2010). Forming characteristics analysis of the cross-section of axially inner grooved copper tube. The International Journal of Advanced Manufacturing Technology, 47, 1023-1031.

[5] Ma, Z. E. (1993). Optimal angle of attack in tube spinning. Journal of Materials Processing Technology, 37(1-4), 217-224.

[6] Li, M., Zhang, S. H., & Kang, D. (2005). Research on selecting working angle in ball spinning. International journal of vehicle design, 39(1-2), 73-79.

[7] Jiang, S., Ren, Z., Li, C., & Xue, K. (2009). Role of ball size in backward ball spinning of thin-walled tubular part with longitudinal inner ribs. Journal of materials processing technology, 209(4), 2167-2174.

[8] Rotarescu, M. I. (1995). A theoretical analysis of tube spinning using balls. Journal of materials processing technology, 54(1-4), 224-229.

[9] Zhang, Y. Q., Jiang, S. Y., Zheng, Y. F., & Zhao, L. H. (2010). Finite element simulation of backward ball spinning of thin-walled tube with longitudinal inner ribs. Advanced Materials Research, 97, 111-115.
[10] Chunjiang, Z., Jie, X., Xiaodong, H., Lianyun, J., Jiefeng, L., & Chen, W. (2017). The analytical model of ball-spinning force for processing an annular groove on the inner wall of a steel tube. The International Journal of Advanced Manufacturing Technology, 91, 4183-4190.
[11] Zeng, X., Fan, X. G., Li, H. W., Zhan, M., Zhang, H. R., Wu, K. Q., ... & Li, S. H. (2020). Die filling mechanism in flow forming of thin-walled tubular parts with cross inner ribs. Journal of Manufacturing Processes, 58, 832-844.
[12] Kuss, M., & Buchmayr, B. (2016). Damage minimised ball spinning process design. Journal of materials processing technology, 234, 10-17.
[13] Zhang, G. L., Zhang, S. H., Li, B., & Zhang, H. Q. (2007). Analysis on folding defects of inner grooved copper tubes during ball spin forming. Journal of materials processing technology, 184(1-3), 393-400.
[14] Shuyong, J., & Zhengyi, R. (2008). Analysis of mechanics in ball spinning of thin-walled tube. Chin J Mech Eng, 21(1), 25-30.
[15] Ahmed, K. I. (2011). A new ball set for tube spinning of thin-walled tubular parts with longitudinal inner ribs. JES. Journal of Engineering Sciences, 39(1), 15-32.
[16] Kassar, M., Ahmed, K., ElSheikh, M., & El-Abden, S. (2022). Tube Spinning Using Functionally Graded Ballizing. Available SSRN, 3977528.
[17] Edriys, I. I., & Fattouh, M. (2013). Characteristics of Finished Holes By Ballizing Process. ERJ. Engineering Research Journal, 36(4), 403-415.
[18] Lai, M. O., & Nee, A. Y. C. (1989). The effect of several finishing processes on the fatigue resistance of hole surfaces.
[19] Dyl, T. (2017). The numerical and experimental analysis of ballizing process of steel tubes. Archives of Metallurgy and Materials, 62(2A), 807-814.
[20] Dyl, T. (2017). The Numerical Analysis of the Ballizing Process. Scientific Journal of Gdynia Maritime University, (100), 63-75.
[21] Fattouh, M. (1989). Some investigations on the ballizing process. Wear, 134(2), 209-219.
[22] El-Abden, S. Z., Abdel-Rahman, M., & Mohamed, F. A. (2002). Finishing of non-ferrous internal surfaces using ballizing technique. Journal of materials processing technology, 124(1-2), 144-152.
[23] Kim, N., Kim, H., & Jin, K. (2013). Minimizing the axial force and the material build-up in the tube flow forming process. International Journal of precision engineering and manufacturing, 14, 259-266.
[24] Nee, A. Y. C., & Venkatesh, V. C. (1983). A mathematical analysis of the ball-burnishing process. CIRP annals, 32(1), 201-204.
[25] Nee, A. Y. C., & Venkatesh, V. C. (1984). Dry and lubricated ballizing. Tribology international, 17(1), 25-29.
[26] Upadhyay P. K, Joshi H, Agarwal P. Evaluation of Different Forces for Super Finishing the Internal Surface of Ballizing process. Mat.Sci.Res.India;9(2). Available from: http://www.materialsciencejournal.org/?p=1105
[27] Nee, A. Y. C., & Venkatesh, V. C. (1982). Bore finishing—the ballizing process. Journal of Mechanical Working Technology, 6(2-3), 215-226.
[28] Khodadadi, M., Khalili, K., & Ashrafi, A. (2020). Studying the effective parameters on teeth height in internal gear flowforming process. International Journal of Engineering, 33(12), 2563-2571.
[29] Maximov, J. T., Duncheva, G. V., & Amudjev, I. M. (2013). A novel method and tool which enhance the fatigue life of structural components with fastener holes. Engineering Failure Analysis, 31, 132-143.
[30] Upadhyay P. K, Agarwal P, Ansari A. R. Discussion and Analysis of Ball Rolling (Ballizing) Process with Elastic and Plastic Deformation between Ball and Material. Mat.Sci.Res.India;9(1). Available from: http://www.materialsciencejournal.org/?p=1218.

[31] Abd-Eltwab, A. A., El-Abden, S. Z., Ahmed, K. I., El-Sheikh, M. N., & Abdel-Magied, R. K. (2017). An investigation into forming internally-spline sleeves by ball spinning. International Journal of Mechanical Sciences, 134, 399-410.
[32] Ayman Ali Abd-Eltwab, Essam Khalaf Saied, Ahmed Mohamed Atia, Nouby M. Ghazaly, A.A. Gomaa, Karim Mohamed Atia (2024). Investigation of externally toothed parts forming using ballizing technique. Results in Materials, 24 (2024) 100640. https://doi.org/10.1016/j.rinma.2024.100640.
[33] Bhatt, R. J., & Raval, H. K. (2018). In situ investigations on forces and power consumption during flow forming process. Journal of Mechanical Science and Technology, 32, 1307-1315.
[34] Droge Krafte, K., und Material fluss beim Drucken, T.H. Stuttgart, (1954)
[35] Hayama M., "Theoretical Study of Tube Spinning", Bull. Fac. Eng. Yokohama Univ., Vol. 15, pp. 33-47, (1966)
[36] Ragab K. Abdel-Magied, Emad A. Fahmy, A. El-Sayed M. Hassan, Mohamed N. El-Sheikh, Essam K. Saied and Ayman A. Abd-Eltwab, "An Investigation into Forming Externally Toothed Parts using Novel Tool based on Rotary Forging Technique." International Journal of Advanced Science and Technology, ISSN: 2005-4238 IJAST, Vol. 29, No.03, (2020), pp. 2194-2206.
[37] Abd-Eltwab, A.A., Helal, G.I., El-Sheikh, M.N., Saied, E.K., & Atia, A.M. (2023). An Investigation into Conventional Spinning Process Using Ball Shaped Rollers as Forming Tool. Manufacturing Technology Journal, 23(6), 788-800. doi: 10.21062/mft.2023.084.
[38] Abd-Eltwab, A.A., Elsyed Ayoub, W., El-Sheikh, M.N., Saied, E.K., Ghazaly, N.M., & Gomaa, A.A. (2024). An Investigation into Forming of Gears Using Rotary Forging Process. Manufacturing Technology Journal, 24(4), 539-551. doi:10.21062/mft.2024.068.
[39] Abd-Eltwab, A.A., Hamdy, K., ELSheikh, A., Saied, E.K., Ghazaly, N.M., & Gomaa, A.A. (2024). An investigation into production of double wall tube using squeeze Ballizing technique. Journal of Manufacturing Processes, 127 (2024) 545–558. https://doi.org/10.1016/j.jmapro.2024.08.005
[40] Heshmat, M., & Abdelrhman, Y. (2020). ANOVA and regression model of slurry erosion parameters of a polymeric spray paint film. International Journal of Materials Engineering Innovation, 11(3), 198-211.
[41] Astakhov, V. P. (2012). Design of experiment methods in manufacturing: Basics and practical applications. In Statistical and computational techniques in manufacturing (pp. 1-54). Berlin, Heidelberg: Springer Berlin Heidelberg.
[42] Abdelaal, O., Heshmat, M., & Abdelrhman, Y. (2020). Experimental investigation on the effect of water-silica slurry impacts on 3D-Printed polylactic acid. Tribology International, 151, 106410.
[43] Heshmat, M., Maher, I., & Abdelrhman, Y. (2023). Surface roughness prediction of polylactic acid (PLA) products manufactured by 3D printing and post processed using a slurry impact technique: ANFIS-based modeling. Progress in Additive Manufacturing, 8(2), 87-98.
[44] Mahapatra, S., Das, A., Jena, P. C., & Das, S. R. (2023). Turning of hardened AISI H13 steel with recently developed S3P-AlTiSiN coated carbide tool using MWCNT mixed nanofluid under minimum quantity lubrication. Proceedings of the Institution of Mechanical Engineers, Part C: Journal of Mechanical Engineering Science, 237(4), 843-864.
[45] Jena, P. C., Pohit, G., & Parhi, D. R. (2017). Fault measurement in composite structure by fuzzy-neuro hybrid technique from the natural frequency and fibre orientation. JOURNAL OF VIBRATION ENGINEERING & TECHNOLOGIES, 5(2), 123-136.
[46] Jena, P. C., Parhi, D. R., & Pohit, G. (2016). Dynamic study of composite cracked beam by changing the angle of bidirectional fibres. Iranian Journal of Science and Technology, Transactions A: Science, 40, 27-37.
[47] Sahoo, S., Parida, S. P., & Jena, P. C. (2023). Dynamic response of a laminated hybrid composite cantilever beam with multiple cracks & moving mass. Structural Engineering and Mechanics, An Int'l Journal, 87(6), 529-540.

[48] Saraswati, P. K., Sahoo, S., Parida, S. P., & Jena, P. C. (2019). Fabrication, characterization and drilling operation of natural fiber reinforced hybrid composite with filler (fly-ash/graphene). Int. J. Innov. Technol. Explor. Eng, 8, 1653-1659.
[49] Parida, S. P., Sahoo, S., & Jena, P. C. (2024). Prediction of multiple transverse cracks in a composite beam using hybrid RNN-mPSO technique. Proceedings of the Institution of Mechanical Engineers, Part C: Journal of Mechanical Engineering Science, 238(16), 7977-7986.
[50] Jena, P. C., Parhi, D. R., & Pohit, G. (2019). Dynamic investigation of FRP cracked beam using neural network technique. Journal of Vibration Engineering & Technologies, 7, 647-661.
[51] Sahoo, S., & Jena, P. C. (2023). Damage detection using recurrent neural network in hybrid composite beam. In Advances in Modelling and Optimization of Manufacturing and Industrial Systems: Select Proceedings of CIMS 2021 (pp. 593-603). Singapore: Springer Nature Singapore.
[52] Parida, S. P., & Jena, P. C. (2023). Selective layer-by-layer fillering and its effect on the dynamic response of laminated composite plates using higher-order theory. Journal of Vibration and Control, 29(11-12), 2473-2488.
[53] Sahoo, S., & Jena, P. C. (2021). Analysis of GFRP cracked cantilever beam using artificial neural network. Materials Today: Proceedings, 44, 1788-1793.
[54] Parida, S. P., Jena, P. C., Das, S. R., Basem, A., Khatua, A. K., & Elsheikh, A. H. (2024). Transverse vibration of laminated-composite-plates with fillers under moving mass rested on elastic foundation using higher order shear deformation theory. Proceedings of the Institution of Mechanical Engineers, Part C: Journal of Mechanical Engineering Science, 238(20), 9878-9888.
[55] Sahoo, S., & Jena, P. C. (2023). Effect of lamina orientation, crack severity, and fillers on dynamic parameters of hybrid composite cantilever beam with double transverse cracks. Materialwissenschaft und Werkstofftechnik, 54(6), 737-750.
[56] Jena, P. C. (2018). Fault assessment of FRC cracked beam by using neuro-fuzzy hybrid technique. Materials Today: Proceedings, 5(9), 19216-19223.
[57] Jena, P. C., Parhi, D. R., Pohit, G., & Samal, B. P. (2015). Crack assessment by FEM of AMMC beam produced by modified stir casting method. Materials Today: Proceedings, 2(4-5), 2267-2276.
[58] Dhupal, D., Panigrahi, D., Rout, S., Bhuyan, R. K., Nayak, S., Jena, P. C., & Das, S. R. (2024). Generation of effusion holes on ultra-high temperature alloy by micro electro-discharge machining process. Surface Review and Letters, 31(02), 2450015.
[59] Pradhan, S., Das, S. R., Jena, P. C., & Dhupal, D. (2022). Investigations on surface integrity in hard turning of functionally graded specimen under nano fluid assisted minimum quantity lubrication. Advances in Materials and Processing Technologies, 8(sup3), 1714-1729.

الملخص العربي

الأجـزاء المسـننة خارجيًـا لهـا دور مهـم للغايـة ولا غنـى عنـه فـي جميـع مجـالات الإنتـاج والتصنيع لأنها تعمل كوسيلة لنقل الحركة والطاقة والقوة في جميع التطبيقات الصناعية، مثل وسائل النقل والطيران والفضاء والمعدات وآلات التشغيل مثل المخرطة والماكينات الاخرى تحتوي جميع الآلات على علبة تروس. لذلك، فهي تحظى باهتمـام متزايـد. يقـدم هـذا البحـث انتاج اجزاء مسننه فى مشوار واحد باداة تشكيل متعدد مستوى بلى التشكيل استنادا الى تقنيـة الكرات الدوارة . تم التحقيق في هذه العمليـة تجريبيـاً ورياضـيًا. كانـت المتغيـرات التـي تـم فحصها تجريبياً في الظروف للكرة ذات المرحلـة الواحـدة هـي: سـرعة دوران القالـب ٣١٥ دورة في الدقيقة ؛ معدل التغذية المحوري، ٠,١٣ مم / دورة ؛ يتم عمق التشكيل بين الكرات والعينة ٥,٥ و ٦,٥ مم الى ثلاث مراحل مـن اداة تشـكيل بأقطـار خارجيـة متدرجـة ومثبتـة على عمود واحد ؛ سمك الأنبوب الأولي هو ٧ و ٨ مم. تم دراسة تأثير هذه المتغيـرات علـى حمل التشكيل ونسبة ملئ تجويف الاسطمبة وجودة القطعة المشكلة، وأظهرت النتائج أن هذه المتغيرات تؤثر على حمل التشكيل ونسبة الملئ وجودة المنتج، وتم اسـتنباط تعبيـر رياضـي للتنبؤ بأحمال التشكيل، ووجد أن النتائج النظريـة تتفـق بشـكل وثيـق مـع التجريبيـة، وأثبتـت النتائج التجريبية نجاح هذه التقنية الجديدة في تشكيل الأجزاء المسننة.